Hindawi
Advances in Civil Engineering
Volume 2018, Article ID 4064362, 9 pages
https://doi.org/10.1155/2018/4064362

Research Article

EM-Based Monitoring and Probabilistic Analysis of Prestress Loss of Bonded Tendons in PSC Beams

Zheheng Chen[1,2] **and Shanwen Zhang**[1]

[1]*School of Civil Engineering, Southeast University, Nanjing 210096, China*
[2]*Key Laboratory of Concrete and Prestressed Concrete Structure, Ministry of Education, Southeast University, Nanjing 210096, China*

Correspondence should be addressed to Zheheng Chen; zhehengchen0215@seu.edu.cn

Received 12 July 2018; Accepted 4 September 2018; Published 23 September 2018

Academic Editor: Luigi Di Sarno

The prestress level is a key factor of prestressed concrete (PSC) beams, affecting their long-term serviceability and safety. Existing monitoring methods, however, are not effective in obtaining the force or stress of embedded tendons. This paper investigates the feasibility of elastomagnetic (EM) sensors, which have been used for external tendons, in monitoring the long-term prestress loss of bonded tendons. The influence of ambient temperature, water, eccentricity ratio, plastic duct, and cement grouts on the test results of EM sensors is experimentally examined. Based on the calibrated EM sensors, prestress loss of a group of PSC beams was monitored for one year. In order to further consider the high randomness in material, environment, and construction, probabilistic analysis of prestress loss is conducted. Finally, the variation range of prestress loss with a certain confidence level is obtained and is compared with the monitored data, which provides a basis for the determination of prestress level in the design of PSC beams.

1. Introduction

Prestressed concrete (PSC) beams have been widely used in highway and railway bridges, in which the effective prestress is one key factor influencing the bridge serviceability and safety. However, it is well known that the time-dependent prestress loss is a very complex process, influenced by inherent material properties, external loads or environmental effects, and construction details. [1]. Moreover, there are abundant uncertainties in such a process [2], resulting in difficulties in accurate prediction on prestress loss. As a result, excessive deflections and cracks are often observed in practice [3–6], which highlights the importance of improved design of prestress level of PSC beams.

In order to learn the authentic status of prestress loss in existing PSC beams, various long-term monitoring measures have been investigated. The vibrating wire strain gauges (VWSGs) can obtain the prestress loss due to shrinkage and creep of concrete [7–10], while they would not monitor the loss of stress relaxation. Similar problem exists when the optical fiber sensing is used [11, 12]. Due to the friction or bond of concrete, the stress along the tendon usually changes, and load cell at the beam ends can only obtain the total loss of prestress [13]. As to traditional resistance strain gauges, they are usually adhered to the surface of PT steels in the plastic corrugated pipes, while the narrow working space and the moisture may seriously affect the survival of gauges and their working performance. The elastomagnetic (EM) sensing is a nondestructive and noncontact monitoring technique that is based on the magnetic-elastic effects of ferromagnetic material [14]. At present, it has been usually used in stress monitoring of external tendons (i.e., unbonded tendons), such as the stayed cables, suspenders, and external tendons of PSC bridges, as shown in Figure 1. However, the application of EM sensing in bonded tendons requires further investigation due to the possible influence of plastic duct and cement grouts on measurement results.

In this paper, the feasibility of elastomagnetic (EM) sensors in monitoring the long-term prestress loss in bonded tendons is experimentally investigated, and the influence of

(a) (b) (c)

Figure 1: EM sensors used for the stress monitoring of external cables. (a) For stayed cables. (b) For suspenders. (c) For external tendons.

ambient temperature, water, eccentricity ratio, plastic duct, and cement grouts on the test results is discussed. Based on the calibrated EM sensors, prestress loss of two PSC beams was monitored for one year. In order to further consider the high randomness in material, environment, and construction, probabilistic analysis of prestress loss is conducted based on the prediction model that can take into account the influence of nonprestressed steels and interaction among concrete creep, shrinkage, and steel relaxation. Finally, the variation range of prestress loss with a certain confidence level is obtained and is compared with the monitored data, which provides a basis for rational determination of prestress level in the design of PSC beams.

2. Elasto-Magnetic (EM) Sensing

2.1. Principle of EM Sensing. The EM sensor is a nondestructive and noncontact test method, based on the inherent magnetic-elastic effect in the ferromagnetic material. The change in tension force can be obtained by measuring variations in magnetic permeability of prestressed tendons. As shown in Figure 2, the EM sensor consists of two layers of coils (i.e., the excitation and measurement coils) and the temperature sensor, and Figure 3 shows the measuring principle of EM sensor. The steel tendon will be magnetized when the pulse current flows into excitation coil, and pulsed magnetic field can be generated along the steel tendon. Due to electromagnetic induction, voltage is induced in the measurement coil. Magnitude of the induced voltage depends on the magnetic permeability of steel tendon, which is a function of the stress of the tendon, as shown in Equation (1).

The increment of magnetic permeability of the test specimen with respect to its zero stress state is expressed as follows:

$$\mu = 1 + \frac{S_0}{S_f}\left(\frac{V_{out}}{V_0} - 1\right), \tag{1}$$

where V_0 represents the integral value of voltage when there is no test specimen in the EM sensor, V_{out} denotes the integral value of voltage when there is a test specimen, S_0 is the area of section surrounded by measurement coil, and S_f represents the net area of test specimen. The relationship between tension force and the increment of magnetic permeability can be expressed by the following equation:

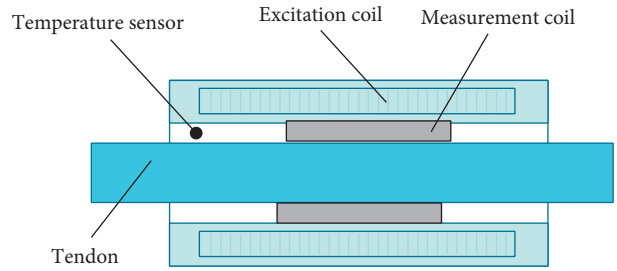

Figure 2: Configuration of an EM sensor.

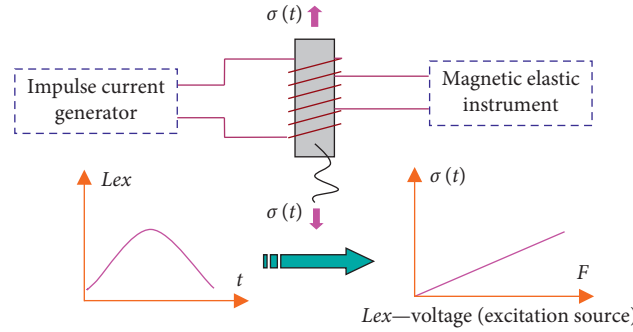

Figure 3: Measuring principle.

$$f = C_0 + C_1\mu + C_2\mu^2 + C_3\mu^3, \tag{2}$$

where C_0,C_1, C_2, and C_3 are the coefficients of the cubic polynomials, which can be obtained from the calibration tests of EM sensors. Note that the effect of temperature on the magnetic permeability of ferromagnetic materials should be eliminated during the test, and the variation of magnetic permeability due to temperature effect can be modified by the following formula:

$$\mu(f,T) = \mu(f,T_0) + \alpha(T - T_0), \tag{3}$$

where T and T_0 are the test and the reference temperatures, respectively; $\mu(f,T)$ and $\mu(f,T_0)$ are the increments of magnetic permeability corresponding to the two temperatures; and α is the slope of the magnetic permeability vs. temperature relationship.

2.2. Tests on Influencing Factors of EM Sensor. A group of tests were designed to investigate the factors that may influence the performance of EM sensors. First, the influence of ambient temperature on the tests is experimentally investigated. It is known that the permeability of steel specimens changes with the temperature, while the slope of the relationship between the permeability and stress of steel specimens does not change within −30°C to 60°C [15]; therefore, the temperature calibration is carried out under the zero stress condition. In this study, a steel tendon with zero stress and the diameter of 15.24 mm was inserted in one EM sensor (type CCT43B) with the inner diameter of 43 mm, and they were put in a constant temperature box. The temperature started from 20°C and gradually rose to 50°C with an increment of 5°C. Under each temperature, the specimen was kept inside a temperature box for 1 hour before reading the relative magnetic permeability. The function curve of temperature and permeability is obtained, as shown in Figure 4, where linear relationship between temperature and the relative magnetic permeability is observed with the slope of 0.013.

Secondly, the influence of ambient media on the test results was analyzed, where there were four tests. In the test No. 1, the EM sensor was put in air while in the test No. 2, the EM sensor was immerged in water. No specimens were put inside the sensor in the test Nos. 1 and 2. In the test Nos. 3 and 4, the EM sensors were put in air and immerged in water, respectively, with a steel tendon inside the sensor. In each test, the integral voltages were measured for six times, and the ambient temperature was 16°C. According to the test results in Table 1, the integral voltages in water are almost the same as those in air, no matter there are steel specimens inside or not, showing that the water has no influence on the measurement results.

In addition, the inner diameter of EM sensor is usually significantly larger than the specimen; therefore, in some cases the specimen is difficult to be completely located in the centroid of EM sensor. To investigate the influence of eccentricity, another three tests were conducted, as shown in Figure 5. In test No. 5, the steel tendon with the diameter of 15.24 mm was located in the centroid of the sensor; in test No. 6 the tendon was located at the lowest position in the sensor (having the largest vertical eccentricity) and in test No. 7 the tendon was inclined. The test results presented in Table 2 indicate that the value in test No. 6 is lower than those in tests No. 5 and 7, showing that the eccentricity has certain influence on the measurement results; therefore, the sensor should avoid excessive eccentricity when used.

In practice, the steel tendons are usually embedded in corrugated ducts with or without grouts. In order to study the influence of tendon ducts and grouts, the test No. 8 and test No. 9 were conducted, where in the test No. 8, there is a corrugated plastic duct outside the tendon and in the test No. 9, the duct was grouted. As compared with the results in the test No. 3, the two tests in Table 3 are almost the same. Therefore, the corrugated ducts and cement grouts, being nonmetal materials, do not have any influence on the measurement results of EM sensor.

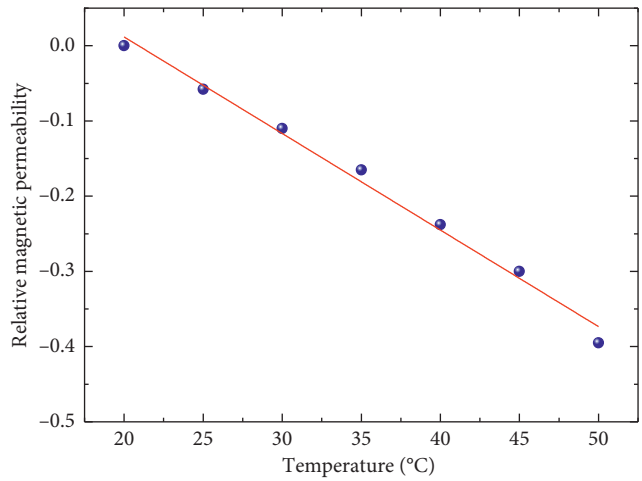

Figure 4: Temperature vs. permeability relationship.

Table 1: Integral voltages of specimen with various ambient media (unit: voltage).

Test	Serial number of measurement						Mean
	1	2	3	4	5	6	
1	526.7	526.3	526.7	527.0	526.9	527.0	526.8
2	526.6	526.7	526.3	526.7	526.9	526.5	526.6
3	641.0	640.7	640.8	640.6	641.2	640.6	640.8
4	640.9	640.4	641.1	640.5	640.7	640.8	640.7

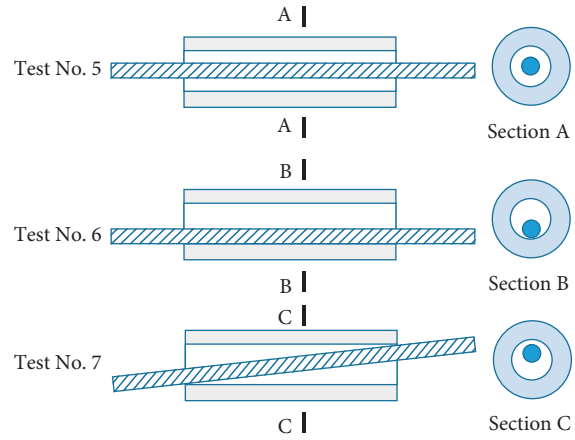

Figure 5: Positions of tendon in the sensor.

Table 2: Integral voltages of specimen with various eccentricities (unit: voltage).

Test	Serial number of measurement						Mean
	1	2	3	4	5	6	
5	640.9	641.2	640.5	640.4	640.8	640.5	640.7
6	637.6	637.4	637.4	637.1	637.2	636.9	637.3
7	640.4	640.6	640.8	640.1	640.5	639.9	640.4

Finally, the relative magnetic permeability of the EM sensor was measured under various levels of loads, as illustrated in Figure 6, where the relative magnetic

Table 3: Integral voltages of specimens with duct and grout (unit: voltage).

Test	Serial number of measurement						Mean
	1	2	3	4	5	6	
8	640.4	640.9	640.7	640.5	640.2	640.1	640.5
9	640.2	640.4	640.5	640.0	640.4	640.0	640.3

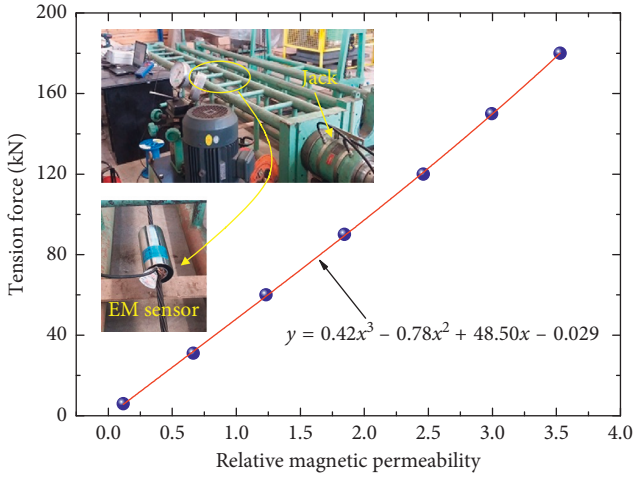

Figure 6: Relative magnetic permeability vs. tension force relationship.

permeability vs. tension force relationship is basically linear, and the cubic polynomial is used to describe the relation.

3. Long-Term Monitoring of Prestress Loss of Bonded Tendons in PSC Beams

Based on the feasibility of EM sensors in monitoring the long-term prestress loss in bonded tendons, as depicted in Section 2, a series of tests were conducted, and two of them are taken for analysis in this paper. The simply supported concrete beams were made using the C55 concrete, which has the 28-day cubic compressive strength of 55 MPa. The beams have a clear span of 4.2 m and a rectangular cross section of 200×300 mm, as shown in Figure 7. High-strength and low-relaxation 1860 grade steel strand was adopted as prestressed reinforcement, and the diameter of the reserved duct was 35.4 mm. The HRB335 grade twisted steel was used as longitudinal main reinforcement, the HPB235 grade round steel with diameter of 8 mm was adopted as transverse stirrups for the rest of the beams, and the stirrup spacing was 150 mm in all beams. The prestressing forces were applied directly to the target values at the age of 30 days. The initial tension forces of PC1 and PC4 are 100.1 kN and 135.9 kN, respectively, which were applied at one end of the beams with load cell installed to control the jacking force. Plain concrete blocks were applied as the secondary dead load at the two 1/3 beam spans immediately after the jacking, each with the weight of 3.125 kN. The detailed design parameters of the beams are shown in [16].

Figure 8 illustrates the time-varying prestress loss of beams PC1 and PC4, monitored using EM sensors, where the development of prestress loss with time is similar in pattern to concrete creep and shrinkage. The long-term loss developed rapidly in the early monitoring period, and the growth rate of time-varying loss becomes gradually gentle after about 250 days. Due to the higher initial tension of the tendon in PC4, the long-term loss at 1/3 section of PC4 is 62.9 MPa after one year of monitoring, which is about 1.42 times of that of PC1. In addition, the monitored long-term loss exhibits some fluctuations during the whole monitoring period, which is due to the variation of environmental factors such as humidity.

4. Probabilistic Analysis of Long-Term Prestress Loss of Bonded Tendons

4.1. Probabilistic Model of Long-Term Prestress Loss. Based on the method of age-adjusted effective modulus [17], the random prediction model for long-term prestress loss which takes into account nonprestressed steels and interaction among concrete creep, shrinkage, and steel relaxation is expressed in Equation (4), of which the detailed derivation can also be found in [16]:

$$\sigma_p(t) = \frac{A_p \sigma_{c,p}(\tau)\varphi(t,\tau) + B_p E_p \varepsilon_{sh} + C_p \overline{\sigma}_{pr}(t)}{D_p}, \tag{4}$$

where $n = \sigma_{c,s}(\tau)/\sigma_{c,p}(\tau)$, $\alpha = E_{sp}/E_c(\tau)$, $E_{sp} = (E_s + E_p)/2$, $\varphi(t,\tau) = \psi_1 \varphi_0 \beta_c(t,\tau)$, and $\varepsilon_{sh} = \psi_2 \varepsilon_{sh0} \beta_s(t,\tau)$; $\sigma_{c,p}(\tau)$ and $\sigma_{c,s}(\tau)$ represent the instantaneous elastic stresses of concrete at the centroids of PT tendons and nonprestressed steels at first loading time, respectively; E_s, E_p, and $E_c(\tau)$ are the elastic moduli of nonprestressed steels, PT tendons, and concrete, respectively; $\varphi(t,\tau)$ and ε_{sh} are the creep coefficient and shrinkage strain and aging coefficient at time t, respectively.

In order to consider the uncertainties in creep model and shrinkage model, two coefficients, ψ_1 and ψ_2, are adapted in this study. For the CEB-FIP90 model, the statistical characteristic values of ψ_1 and ψ_2 can be taken as $E(\psi_1) = 1$, $V(\psi_1) = 0.339$ and $E(\psi_2) = 1$, $V(\psi_2) = 0.451$ [18], respectively; φ_0 is the nominal creep coefficient; $\beta_c(t,\tau)$ is the coefficient to describe the development of creep with time; ε_{sh0} is the nominal shrinkage strain; $\beta_s(t,\tau)$ is the coefficient to describe the development of shrinkage with time; $\overline{\sigma}_{pr}(t)$ is the reduced relaxation loss and equals to $\lambda_r \sigma_{pr}(t)$; λ_r denotes the reduction factor, and a value of 0.75 [19] is adopted in this study, and the calculation method of intrinsic relaxation, $\sigma_{pr}(t)$ by Youakim et al. [20], is adopted in this paper.

The coefficients A_p, B_p, C_p, and D_p are as shown in the following equation:

$$\begin{cases} A_p = \alpha\left[1 + \alpha\rho_s r_{s,s}(1+\chi\varphi) - n\alpha\rho_s r_{p,s}(1+\chi\varphi)\right], \\ B_p = 1 + \alpha\rho_s(1+\chi\varphi)\left(r_{s,s} - r_{p,s}\right), \\ C_p = 1 + \alpha\rho_s r_{s,s}(1+\chi\varphi), \\ D_p = 1 + \alpha(1+\chi\varphi)\left(\rho_s r_{s,s} + \rho_p r_{p,p}\right), \end{cases} \tag{5}$$

where ρ_s and ρ_p represent the ratio of nonprestressed steels and PT tendons, respectively; $r_{i,j} = 1 + e_i e_j / r_c^2$, where i or j

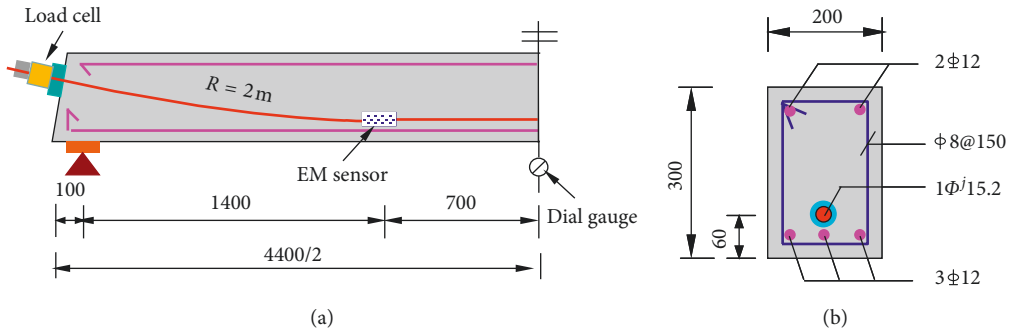

Figure 7: Structural dimensions and sensor layout of beams PC1 and PC4. (a) Profile. (b) Cross section (at midspan).

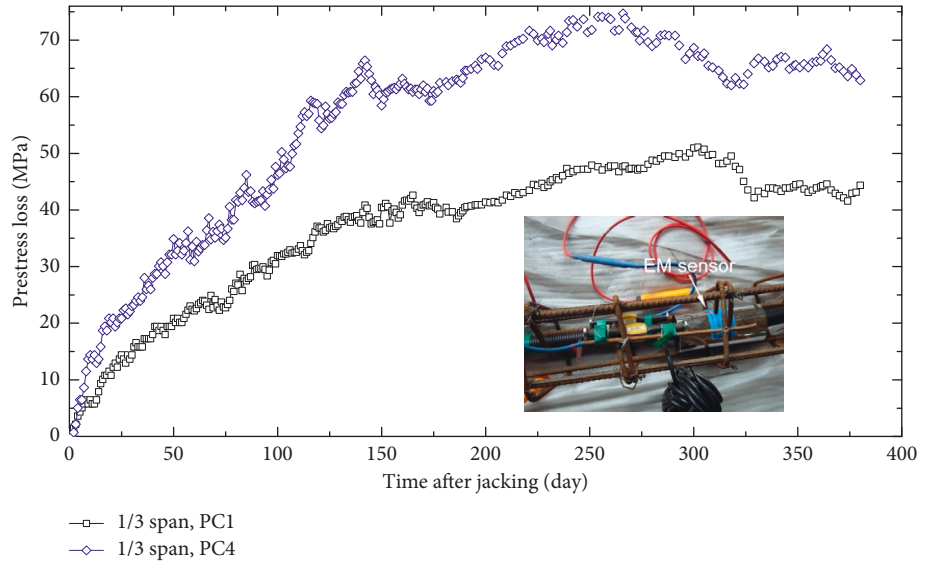

Figure 8: Long-term prestress losses of beams PC1 and PC4.

represents the nonprestressed steels (s) or PT tendons (p), and e_s and e_p are the eccentricity of nonprestressed steels and the PT tendons with respect to the centroid of concrete, respectively, and r_c is the radius of gyration of the concrete section; χ is the aging coefficient, which varies between 0.6 and 1.0 [21], and the value of 0.8 is adopted in this study for simplicity.

4.2. Statistical Properties of Random Parameters. The mechanism and influence factors of concrete shrinkage and creep are very complicated, and there are usually large deviations between the predicted and measured values of effects of concrete creep and shrinkage. There are many reasons leading to this phenomenon, and one of the main reasons is that the selected prediction model of shrinkage and creep itself is not perfect. At present, most of the shrinkage and creep models are the empirical formulas obtained through statistical regression based on experimental data, and the models themselves have the fitting errors; therefore, model uncertainty factors are used to describe the deviation. Some scholars have conducted extensive research on uncertainty of shrinkage and creep models [22–24]. For the CEB-FIP90 model, the statistical characteristic values of the model uncertainty factor are shown in Table 4.

Meanwhile, it is necessary to consider the randomness of parameters in the prediction model during the analysis of long-term loss of prestress, where the concrete compressive strength, ambient relative humidity, and loading age are treated as random variables. According to [25], the concrete strength used in this study follows the normal distribution with a mean value of 63.9 MPa and a coefficient of variation (COV) of 0.089. The ambient relative humidity is another significant factor which influences the time-varying effects of concrete structure, and the relative humidity in the laboratory exhibits seasonal fluctuations. According to the meteorological data of Nanjing, the probability density function (PDF) of ambient relative humidity is obtained, which follows a normal distribution with the mean value of 75% and the COV of 0.161. Other random factors include the density of concrete, initial loading age, elastic modulus of prestressing steel, areas of nonprestressed, and prestressed steel, which are described

Table 4: Statistical properties of random variables.

Random variables	Unit	Mean	COV	Distribution	Sources
Uncertainty factor for creep model, ψ_1	—	1	0.339	Normal	[18]
Uncertainty factor for shrinkage model, ψ_2	—	1	0.451	Normal	[18]
Concrete strength, f_{cu}	MPa	63.9	0.089	Normal	[25]
Density of concrete, DW	kN/m^3	25.5	0.046	Normal	[26]
Initial stress in steel, σ_p	MPa	723 (PC1) 977 (PC4)	0.020	Normal	[27]
Annual relative humidity, RH	%	75.0	0.161	Normal	Observed
Initial loading age, t_0	d	30	0.110	Uniform	Assumed
Elastic modulus of prestressing steel, E_p	MPa	1.95×10^5	0.060	Normal	[28]
Area of nonprestressed steel, A_s	mm^2	565.5	0.035	Normal	[29]
Area of prestressed steel, A_p	mm^2	140	0.0125	Normal	[30]

in Table 4. The geometric sizes of specimens are treated as design constants due to its minor variation. In order to facilitate stochastic analysis, random variables are assumed to be independent of each other.

4.3. Probabilistic Analysis and Discussion. According to the probabilistic model in Section 4.1 and the random factors in Table 4, probabilistic analysis of long-term prestress loss in beams PC1 and PC4 is carried out using the Latin hypercube sampling technique (5000 samples), and the time-varying PDFs are obtained, as shown in Figure 9. It can be seen that the PDFs of long-term prestress loss approximately follow the normal distribution at different ages, and the probability density curves gradually become flat as time goes by, indicating that at the same confidence level, the width of confidence interval of long-term prestress loss becomes larger. As presented in Figure 10, the standard deviation (SD) of long-term loss increases continuously in each calculation condition from 1 month to 30 years after jacking, which shows that the discreteness of prestress loss due to the variation of influencing parameters gradually becomes larger with time, and the increase is most significant in the first ten years.

As shown in Figure 11, the measured long-term loss exhibits some fluctuations during the whole monitoring period, due to variations of ambient temperature and humidity. Although the test results of PC1 are basically consistent with the mean values of stochastic analysis, for PC2, the differences between test results and mean analyzed results become larger, which is due to the uncertainties in analysis of time-varying effect. Note that the mean values of prestress loss are usually adopted in structural design, which might underestimate their actual values and lead to unsafe design. Considering the prestress loss approximately obeying normal distribution at each time, the 95% confidence interval can be supposed as $[\overline{f}_l(t) - 1.96SD(t), \overline{f}_l(t) + 1.96SD(t)]$, where $\overline{f}_l(t)$ represents the mean value of probability analysis of time-varying loss at time t based on Equation (4), and $SD(t)$ represents the SD of time-varying loss at time t. As shown in Figure 10, during the monitored period, the measured long-term prestress loss for beams PC1 and PC4 are located within the 95% confidence interval of

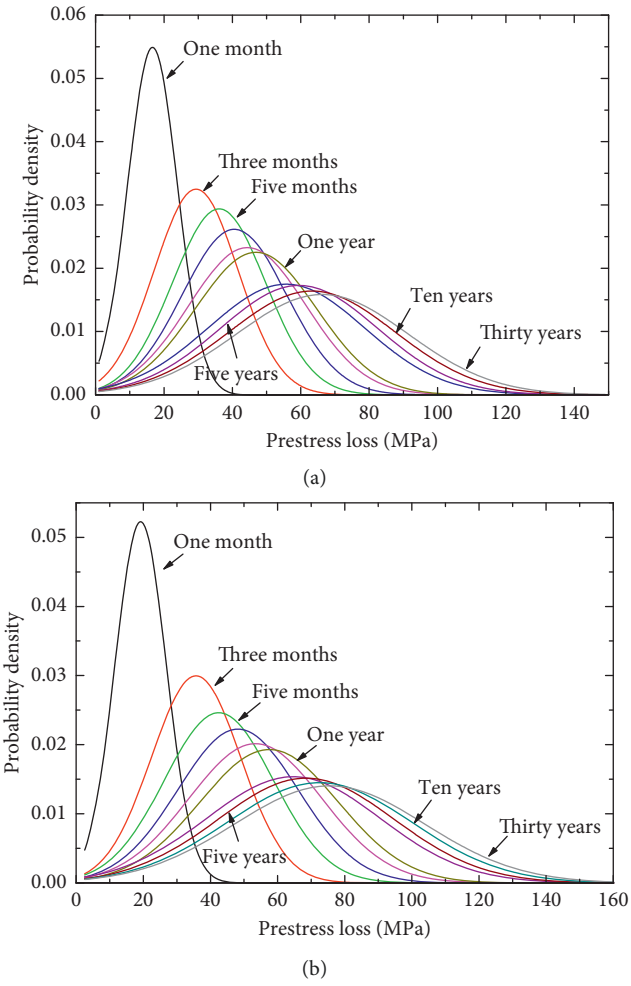

Figure 9: Time-varying PDFs of long-term loss. (a) PC1. (b) PC4.

probabilistic analyses. Taking PC4 as an example, the measured value of long-term loss is 70.6 MPa after about 1 year of monitoring, and the upper bound of 95% confidence interval is 97.1 MPa, which is about 37.5% larger than the measured value. Meanwhile, the width of the confidence interval of long-term loss gradually increased with time, varying from [4.3, 34.1] at one month of monitoring to [13.2, 97.1] at one year of monitoring, which indicates that the discreteness of time-varying loss

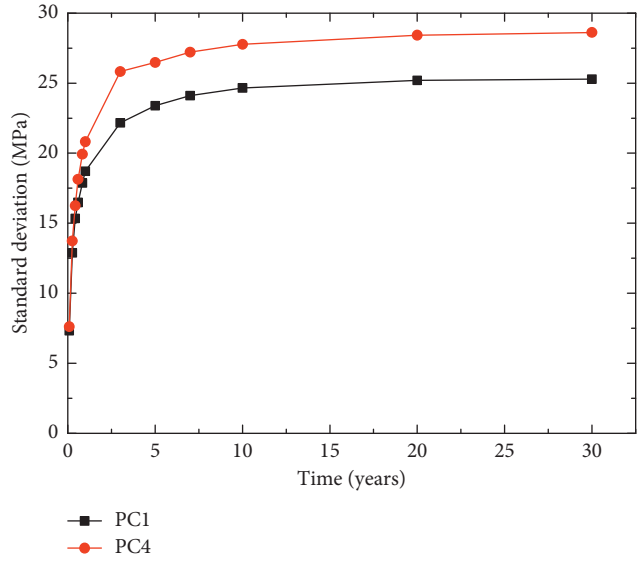

Figure 10: Time-varying SDs of long-term loss.

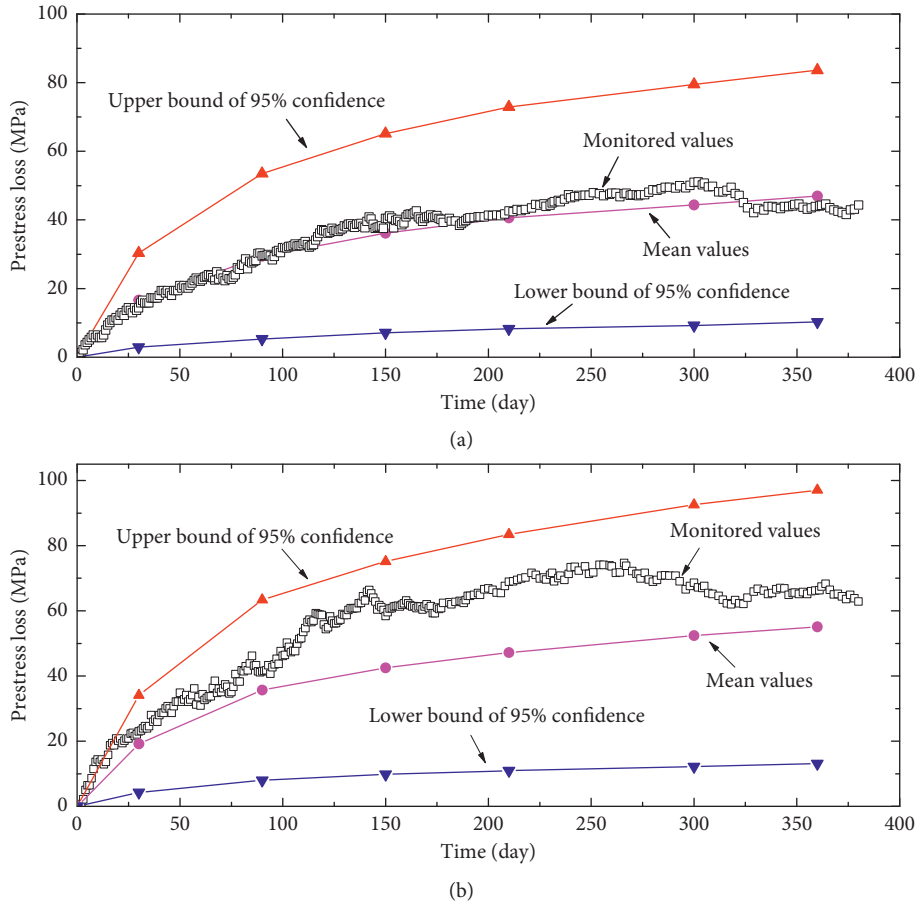

Figure 11: Comparison of probability results of long-term loss with measured values. (a) PC1. (b) PC4.

becomes more obvious due to the larger variability of concrete shrinkage and creep as time goes by. Therefore, it is suggested that the upper bound of 95% confidence interval, instead of the mean value, should be used as the maximum long-term loss which may occur in the actual PSC structures.

5. Conclusions

This paper provides a preliminary investigation on the feasibility of EM sensors in monitoring the long-term prestress loss of bonded tendons. According to the presented study, conclusions are drawn as follows:

(1) The performance tests of EM sensor show that the external media such as water, cement grouting, and plastic duct have no influence on the measurement results, showing that the EM sensor can be well used in steel members bonded in concrete. The temperature has certain influence on the magnetic permeability of the tested specimens, and the correction coefficient can be obtained through temperature calibration at the zero stress state. The eccentricity of the steel specimens relative to the EM sensor has some impact on the test results, and therefore, the steel specimens should be located in the centroid of the EM sensor when it is installed.

(2) The long-term prestress loss due to shrinkage, creep of concrete, and stress relaxation is complicated, and there are significant uncertainties. Therefore, the uncertainty analysis of long-term loss should be carried out in order to make the design of bridges more safe and realistic. Based on the probabilistic analysis model adapted in this study, the probability analyses were conducted, which indicate that the long-term loss of prestress does not reject the normal distribution at each time, and its discreteness gradually become larger with the extension of time. The bandwidth surrounded by the upper and lower bound of 95% confidence interval also gradually increase with time. In addition, the predicted prestress loss in bridge design from deterministic analysis may be significantly different from the authentic monitored values. Therefore, to conduct a safe design, it is suggested that some suitable confidence limits such as 95% should be adopted instead of the mean value.

(3) For the internal prestressed tendons of widespread PSC box girder bridges, the EM sensors installed in the construction stage can be used for the real-time monitoring of effective prestress force in the service process of bridges, which would provide the basis for the long-term performance assessment of the structures. These will be done in the next study.

Data Availability

The data used to support the findings of this study are available from the corresponding author upon request.

Conflicts of Interest

The authors declare that there are no conflicts of interest regarding the publication of this paper.

Acknowledgments

The support from the Open Foundation of National Engineering Laboratory for High Speed Railway Construction under the Grant No. HSR2013029, the Education Department of Jiangsu under Grant No. JHB2012-1, and the Priority Academic Program Development of Jiangsu Higher Education Institutions under the Grant No. CE02-1-38 is gratefully acknowledged.

References

[1] L. A. Caro, J. R. Marti-Vargas, and P. Serna, "Prestressed losses evaluation in prestressed concrete prismatic specimens," *Engineering Structures*, vol. 48, pp. 704–715, 2013.

[2] E. P. Steinberg, "Probabilistic assessment of prestress loss in pretensioned prestressed concrete," *PCI Journal*, vol. 40, no. 6, pp. 76–85, 1995.

[3] R. Malm and H. Sundquist, "Time-dependent analyses of segmentally constructed balanced cantilever bridges," *Engineering Structures*, vol. 32, no. 4, pp. 1038–1045, 2010.

[4] Z. P. Bazant, Q. Yu, and G. Li, "Excessive long-time deflections of prestressed box girders, I: record-span bridge in Palau and other paradigms," *Journal of Structural Engineering*, vol. 138, no. 6, pp. 676–686, 2012.

[5] T. Guo, R. Sause, D. M. Frangopol, and A. Q. Li, "Time-dependent reliability of PSC box-girder bridge considering creep, shrinkage and corrosion," *Journal of Bridge Engineering*, vol. 16, no. 1, pp. 29–43, 2011.

[6] T. Guo, D. M. Frangopol, D. Z. Han, and Y. W. Chen, "Probabilistic assessment of deteriorating prestressed concrete box-girder bridges under increased vehicle loads and aggressive environment," *Journal of Performance of Constructed Facilities*, vol. 25, no. 6, pp. 564–576, 2011.

[7] J. J. Roller, H. G. Russell, R. N. Bruce, and B. T. Martin, "Long-term performance of prestressed, pretensioned high strength concrete bridge girders," *PCI Journal*, vol. 40, no. 6, pp. 48–59, 1995.

[8] T. M. Ahlborn, C. E. French, and C. K. Shield, "High strength concrete prestressed bridge girders: long term and flexural behavior," Report MN/RC–2000–32, Minnesota Department of Transportation, Saint Paul, MN, USA, 2000.

[9] M. Lewis and V. M. Karbhari, "Experimental verification of the influence of time-dependent material properties on long-term bridge characteristics," *SSRP*, vol. 6, p. 20, 2006.

[10] P. J. Barr, B. M. Kukay, and M. W. Halling, "Comparison of prestress losses for a prestress concrete bridge made with high performance concrete," *Journal of Bridge Engineering*, vol. 13, no. 5, pp. 468–475, 2008.

[11] Z. Y. Liang, *Monitoring of a prestressed high performance concrete bridge using an embedded optical fiber sensor system*, Ph.D. Dissertation, New Mexico State University, Las Cruces, NM, USA, 2008.

[12] C. G. Lan, Z. Zhou, and J. P. Ou, "Monitoring of structural prestress loss in RC beams by inner distributed Brillouin and fiber Bragg grating sensors on a single optical fiber," *Structural Control and Health Monitoring*, vol. 21, no. 3, pp. 317–330, 2014.

[13] X. M. Jin, Y. L. Du, B. C. Sun, and X. Y. Li, "Study on optical fiber sensing technology for long-term real time monitoring of prestressed reinforcement," *China Safety Science Journal*, vol. 15, no. 11, pp. 108–112, 2005.

[14] G. D. Wang and M. L. Wang, "The utilities of U-shape EM sensors in stress monitoring," *Structural Engineering and Mechanics*, vol. 17, no. 3–4, pp. 291–302, 2004.
[15] M. L. Wang, G. Wang, and Y. Zhao, "Application of EM stress sensors in large steel cables," *Sensing Issues in Civil Structural Health Monitoring*, pp. 145–154, 2005.
[16] T. Guo, Z. H. Chen, S. Lu et al., "Monitoring and analysis of long-term prestress losses in post-tensioned concrete beams," *Measurement*, vol. 122, pp. 573–581, 2017.
[17] Z. P. Bazant, "Prediction of concrete creep effects using age-adjusted effective modulus method," *ACI Journal Proceedings*, vol. 69, no. 4, pp. 212–217, 1972.
[18] Z. P. Bazant and S. Baweja, "Justification and refinement of model B3 for concrete creep and shrinkage1, statistics and sensitivity," *Materials and Structures*, vol. 28, no. 7, pp. 415–430, 1995.
[19] T. J. Trevino and A. Ghali, "Relaxation of steel in prestressed concrete," *PCI Journal*, vol. 30, no. 5, pp. 82–94, 1985.
[20] S. A. Youakim, A. Ghali, S. E. Hida, and V. M. Karbhari, "Prediction of long-term prestress losses," *PCI journal*, vol. 52, no. 2, pp. 116–130, 2007.
[21] M. F. Granata, P. Margiotta, and M. Arici, "Simplified procedure for evaluating the effects of creep and shrinkage on prestressed concrete girder bridges and the application of European and North American prediction models," *Journal of Bridge Engineering*, vol. 18, no. 12, pp. 1281–1297, 2013.
[22] B. S. Choi, A. Scanlon, and P. A. Johnson, "Monte Carlo simulation of immediate and time-dependent deflections of reinforced concrete beams and slabs," *ACI Structural Journal*, vol. 101, no. 5, pp. 633–641, 2004.
[23] D. Diamantidis, H. O. Madsen, and R. Rackwitz, "On the variability of the creep coefficient of structural concrete," *Materials and Structures*, vol. 17, no. 4, pp. 321–328, 1984.
[24] E. H. Khor, D. V. Rosowsky, and M. G. Stewart, "Probabilistic analysis of time dependent deflections of RC flexural members," *Computers & Structures*, vol. 79, no. 16, pp. 1461–1472, 2001.
[25] T. Guo and Z. H. Chen, "Deflection control of long-span PSC box-girder bridge based on field monitoring and probabilistic FEA," *Journal of Performance of Constructed Facilities*, vol. 30, no. 6, article 04016053, 2016.
[26] GBT50283-1999, *Unified Standard for Reliability Design of Highway Engineering Structures*, China Planning Press, Beijing, China, 1999, in Chinese.
[27] C. G. Gilbertson and T. M. Ahlborn, "A probabilistic comparison of prestress loss methods in prestressed concrete beams," *PCI Journal*, vol. 49, no. 5, pp. 52–69, 2004.
[28] T. Guo, T. Liu, and A. Q. Li, "Deflection reliability analysis of PSC box-girder bridge under high-speed railway loads," *Advances in Structural Engineering*, vol. 15, no. 11, pp. 2001–2011, 2012.
[29] Y. H. Li, W. G. Bao, X. W. Guo et al., *Highway Bridge Structure Reliability and Probability Limit Sate Design*, China Communications Press, Beijing, China, 1997, in Chinese.
[30] A. S. AL-Harthy and D. M. Frangopol, "Reliability assessment of prestressed concrete beams," *Journal of Structural Engineering*, vol. 120, no. 1, pp. 180–199, 1994.